Japanese Journal of Applied Physics

The Japan Society of Applied Physics

REGULAR PAPER

Rapid and scalable fabrication of reduced graphene oxide conducting films by ethanol-assisted thermal annealing of graphene oxide

Japanese Journal of Applied Physics **58**, SIIB07 (2019) **REGULAR PAPER**
https://doi.org/10.7567/1347-4065/ab0ff9

Rapid and scalable fabrication of reduced graphene oxide conducting films by ethanol-assisted thermal annealing of graphene oxide

K. Kanishka, H. De Silva, Hsin-Hui Huang, Seiya Suzuki, and Masamichi Yoshimura*

Graduate School of Engineering, Toyota Technological Institute, 2-12-1 Hisakata, Tempaku, Nagoya 468-8511, Japan

*E-mail: yoshi@toyota-ti.ac.jp

Received December 17, 2018; accepted February 14, 2019; published online June 13, 2019

Fabrication of graphene-based transparent conducting films via thermal annealing of graphene oxide (GO) is under consideration for commercial mass production of graphene-based conducting films as an alternative to high-cost metal oxide-based conducting substrates. Conventional thermal annealing, however, comes with some drawbacks, such as high-temperature annealing along with longer process times and structural damage that hinders the applicability of GO as a transparent conductor. Here we report on a method for fabricating reduced GO-based conducting films at a low temperature (800 °C) in the presence of ethanol as a carbon source to repair the lattice defects. The total process time is less than 1 h. The results confirm that rapid annealing in an ethanol atmosphere is an effective roll-to-roll method which reduces the thermal load on the device used. It is also found that ethanol plays an important role in repairing the lattice defects, thereby lowering the resistance to a great extent.

Supplementary material for this article is available online

1. Introduction

There is a race to find suitable transparent conducting electrodes (TCEs) to replace current metal oxide-based electrodes, such as those using indium tin oxide (ITO). Indium metal is expensive ($2–30 per m^2 for coating with 90% transparency) and scarce, and the preparative methods such as sputtering and electroplating can be costly.[1] In addition, ITO is a brittle crystalline material and hence cannot be used in the same way as flexible TCEs.[2] The minimum standard for a substitutional material is a sheet resistance (R_s) $<100\,\Omega\,sq^{-1}$ coupled with transparency of over 90% in the visible.[1] The graphene sector shows constant progress in the field of TCEs as a result of it being a two-dimensional material with high charge carrier mobility and good optical transmittance, making it the best alternative material to replace expensive and scarce In-based electrodes.[3]

Despite the remarkable electrical and mechanical properties inherent in graphene, there are some barriers to be overcome before graphene can be used in real-life applications. Much effort and high capital expenditure are necessary to fabricate high-quality graphene through chemical vapor deposition (CVD) and epitaxial growth, which is not appropriate for large-scale production.[4,5] As a result, synthesis of graphene by the reduction of graphene oxide (GO) is becoming the most feasible method for graphene synthesis on an industrial-scale.[6] Graphene synthesized via this method is more precisely known as reduced graphene oxide (RGO) to distinguish it from pristine graphene.

As the name implies, GO is a highly oxidized form of graphene. Thus, many oxygen-containing functional groups will be incorporated into the lattice structure, creating many defect sites on the plane.[7,8] These functionalities impart good dispersibility of GO in water, resulting in processable single-layered sheets.[9] Several different ways of fabricating large-area GO films on substrates have been reported so far: for example, spin-coating, dip-coating, drop casting, layer-by-layer deposition, the Langmuir–Blodgett method and interfacial self-assembly.[10] Of these methods, spin-coating is the most often used and is the easiest method for preparing GO films of a few nanometers thick, which permits the fabrication of conductive RGO films.[11] The lattice defects and oxygen-containing functionalities present in GO make it an insulator. Many attempts have been made to synthesize RGO, either by chemical reduction or thermal annealing of GO or a combination of both, to resemble pristine-type graphene, or at least to attain better conducting properties closer to those of pristine graphene.[12] Moreover, doping of graphene by $FeCl_3$, $AuCl_3$, $SOCl_2$, etc, and encapsulation with polymers have also been reported as methods to obtain highly conductive RGO films.[11,13] To date, high-temperature annealing is the only method that can remove almost all oxygen-containing groups while repairing defects in GO.[14] However, there are some points to be taken into account when annealing GO. If annealing is conducted with a sudden temperature increment, in addition to the deoxygenation and exfoliation of GO sheets the graphitic structure can be damaged, creating more defects or lattice vacancies due to the high pressure created between sheets (130 MPa is generated at 1000 °C).[15] This damage is irreversible and affects the electronic properties of the RGO sheets. To avoid excess damage to the graphitic structure by rapid evolution of CO, CO_2 and H_2O, the initial heating from room temperature must be done gradually ($<10\,°C\,min^{-1}$) with a holding temperature.[9] This makes the total process time-consuming, and large amounts of energy are needed for high-temperature annealing. Low-temperature annealing (<500 °C) cannot remove the majority of the functional groups, hence temperatures above at least 750 °C are necessary for better deoxygenation.[16] However, annealing at high temperatures such as 2000 °C is not suitable for all types of substrates.[12] In order to transform GO into pristine graphene by repairing the defects in the graphitic structure, deoxygenation by annealing either in an inert or a H_2-containing environment in the presence of a carbon source has been reported.[17–22] This is done under moderate to high annealing temperatures adopting the conditions used in synthesis of pristine graphene or carbon nanotubes via CVD. Restoration of the graphitic structure during thermal annealing in the presence of ethanol (EtOH) has shown more promising results for the preparation of highly crystalline and conducting RGO films.[19] However, these results were obtained

by annealing either at a very high temperature (2000 °C) or a longer annealing time (3 h).[23] For fabrication of TCEs, temperatures below 900 °C are suitable bearing in mind the thermal stability of the substrates and that long fabrication times are both time- and energy-consuming.[9] Hence, it is necessary to find much better and practical reduction schemes for fabricating conducting and transparent RGO films that satisfy both the substrate requirements and those of industrial-scale fabrication.

The present work demonstrates the fabrication of conducting RGO films by EtOH-assisted annealing at a moderate temperature of 800 °C in less than 1 h using a simple CVD device. This rapid thermal treatment allows the fabrication of conducting RGO films without any noticeable structural damage to the GO sheets.

2. Experimental methods

2.1. Fabrication of GO films

GO was synthesized according to a previously reported method.[22] A stable dispersion of GO (0.2 mg ml^{-1}) was prepared by dispersing dry GO in deionized water. Two types of substrates, SiO_2 (50 nm)/Si and quartz, were used to fabricate the conducting films. Both substrates were cleaned by ultrasonication using acetone and EtOH, and hydroxylated by UV/O_3 treatment. Silane functionalization was done by placing the substrates in a solution of 2% 3-aminopropyltriethoxysilane in toluene for 1 h. Later, the substrates were rinsed with toluene and EtOH, respectively. GO was spin-coated on the substrates at a rate of 4000 rpm while dropping 10 μl of GO per droplet to get samples with different thicknesses (corresponding to total GO loading volumes of 70–1400 μl). All samples were vacuum dried before annealing. To measure the thickness, after spin-coating the GO a slight scratch was made using a toothpick without damaging the underlying substrate. Additionally, to show the effect of EtOH in restoration, two samples were prepared by spin-coating 2 μl of GO on SiO_2 (50 nm)/Si substrates so that a few flakes of GO were deposited; one was annealed with EtOH and the other without EtOH.

2.2. Ethanol-assisted thermal annealing of GO films

Annealing was done in a simple commercial CVD set-up (Microphase MPCNT-Basic). The ceramic cup containing 10 ml of EtOH was placed below the carbon heater and the sample was kept on the carbon heater. Chamber pressure was maintained at 10 kPa by purging with a 3% H_2/Ar gas mixture and evaporating the EtOH. The temperature was increased to 800 °C by increasing the current of the power supply system within about 24 s. The temperature was monitored using a digital infrared thermometer (CHINO IR-AHS0). With the increase in temperature, EtOH started to evaporate. the process being concluded in about 19 min. Total annealing time was fixed to 30 min. Thereafter, the current was reduced to zero and gas purging was stopped. Then the set-up was allowed to come to room temperature while vacuuming to $<$1 kPa.

Additionally, a two-step reduction method (chemical reduction followed by thermal annealing) was carried out in order to study how it would affect the degree of deoxygenation and formation of a conducting film. A detailed methodology and results for this method are given in the online supplementary data.

2.3. Materials characterization

The degree of restoration was monitored by Raman spectroscopy (Renishaw InVia Raman spectroscope). Samples were excited by 532 nm laser with a $\times$50 objective lens. The chemical state of oxygen-containing functionalities was analyzed by X-ray photoelectron spectroscopy (XPS; Ulvac-PHI 5000 Versa Probe II) with an Al Kα X-ray source. Surface topography and film thickness were analyzed by atomic force microscopy (AFM; Bruker Multimode 8) using a Si probe with Al coating (Tap-300, resonance frequency 300 kHz, spring constant 40 N m^{-1}). Transmittance was measured with a Jasco V-650 double-beam UV–visible spectrophotometer. Sheet resistance measurements were carried out by the four-point probe method using a Keithley 2636 system source meter. Samples coated with RGO were patterned with nickel (Ni) contacts by sputtering Ni through a pre-patterned mask. The channel width (W, graphene width) and channel length (L, distance between two electrodes) were measured using an optical microscope and R_s was calculated using the equation $R_s = (RW)/L$, where R is the resistance.[20]

3. Results and discussion

The topography and thickness of the films prepared on SiO_2 (50 nm)/Si substrates before and after annealing were analyzed by AFM. As shown in Fig. 1(a), at lower GO loading volumes from 70–280 μl the GO flakes were clearly resolved up to three to four monolayers, with uncovered regions on the substrate resulting in step heights of 2–3 nm in most areas. As the GO loading volume increased, the uncovered areas were filled and more GO sheets overlapped so that it is difficult to resolve the sheets clearly [Fig. 1(c)]. Figures 1(b) and 1(d) depict the topography of the films obtained after annealing, where the RGO sheets were still observed clearly at 280 μl and dense packing or overlapping occurred at 1400 μl. In our previous report we demonstrated that any noticeable damage on the flakes or delamination of the sheets were not detected with this rapid thermal treatment.[22] Figure 2 illustrates the thickness of the films prepared on SiO_2 (50 nm)/Si substrates measured before and after annealing. With the increase in GO loading the film thickness increases continuously. After annealing, the thickness of all the films is decreased due to the removal of oxygen-containing groups. The number of GO sheets that can be present in any sample was determined taking into account that the thickness of a single sheet of GO is 1 nm.[6] Assuming the number of sheets remains the same after annealing, the thickness of the films was calculated after annealing on the basis that the thickness of a single RGO sheet is 0.4 nm. These results are summarized in Table I. Both calculated and measured thicknesses of RGO sheets are in good agreement, which further affirms that the sheets have not been delaminated. The slight difference can be attributed to the thickness variation that might have been caused by disordered stacking of sheets during spin-coating and the residual oxygen-containing functional groups present among sheets.

The root mean square roughness (R_q) of the prepared films before and after annealing was measured and the results are shown in Fig. 3. With increase in GO loading volume the value of R_q also increases (ranging from 0.58–1.8 nm for 280–1400 μl). Unlike when measuring the R_q of a single GO flake, which may not have any wrinkles on the surface, when

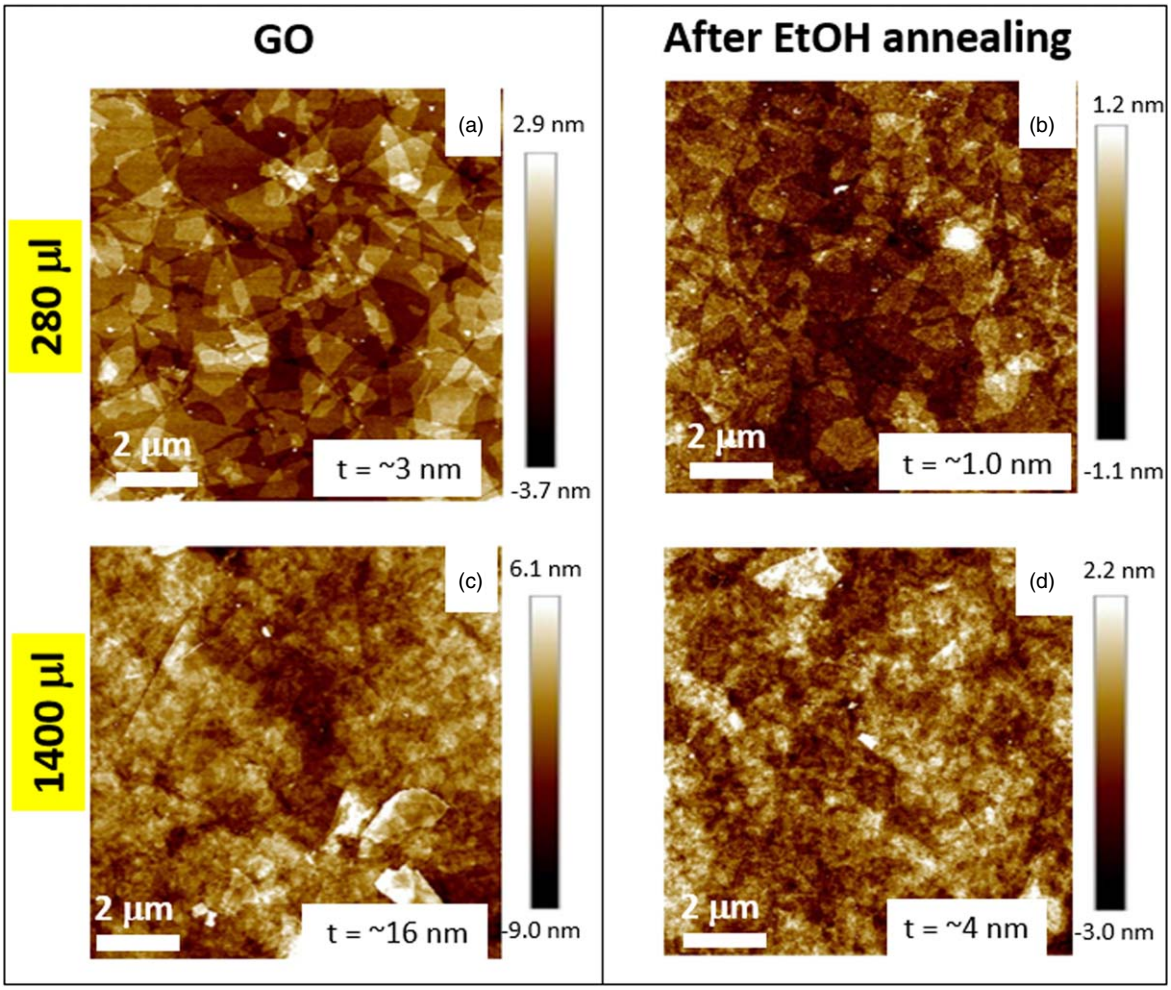

Fig. 1. (Color online) The AFM images of GO and RGO films with different loading volumes: 280 μl film before (a) and after annealing (b), and 1400 μl film before (c) and after annealing (d).

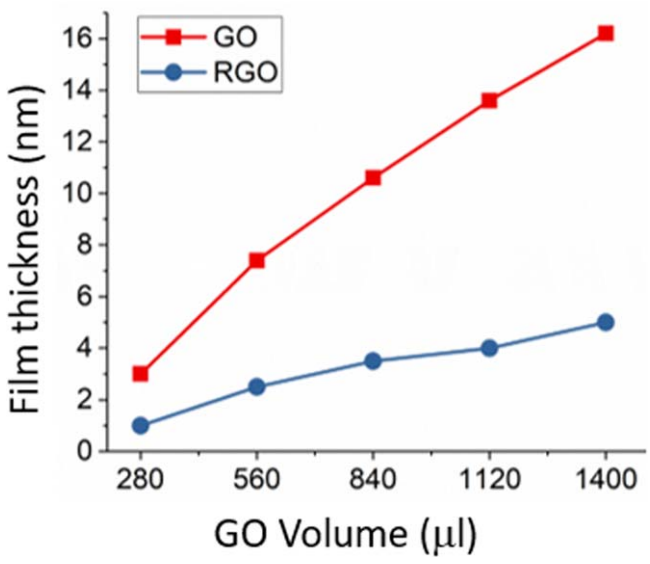

Fig. 2. (Color online) Film thickness before and after annealing of the samples prepared with increasing GO loading volume.

measuring the R_q of GO films one must take into account the wrinkles, folding or any other deformations that occur upon deposition during spin-coating. As a result, the roughness may have increased with the increase in GO loading.

Table I. Thickness of GO (t_{GO}) and RGO (t_{RGO}) films prepared at increasing GO loading volume measured by AFM and the calculated RGO film thickness based on the assumed number of GO sheets.

Sample	t_{GO} (nm)	Assumed no. of sheets	t_{RGO} (nm) (measured)	t_{RGO} (nm) (calculated)
[280]	3.0	3	1.0	1.2
[560]	7.4	7	2.5	2.8
[840]	10.6	10	3.5	4
[1120]	13.6	13	4	5.2
[1400]	16.2	16	5	6.4

However, after annealing, the R_q value of all the films was decreased (ranging from 0.226–0.53 nm for 280–1400 μl). The decrease of the R_q value after annealing is understandable. According to our previous report and other literature,[22,24] when the R_q of GO and RGO flakes is compared, GO has a higher R_q than RGO due to the attached oxygen-containing functional groups and lattice defects. Upon annealing, R_q decreases due to the removal of oxygen-containing functional groups and repair of the lattice defects; hence, the overall roughness of the RGO films will decrease.

Figures 4(a) and 4(b), respectively, represent the high-resolution carbon spectra of GO and RGO films obtained by XPS. GO has four deconvoluted components revealing the

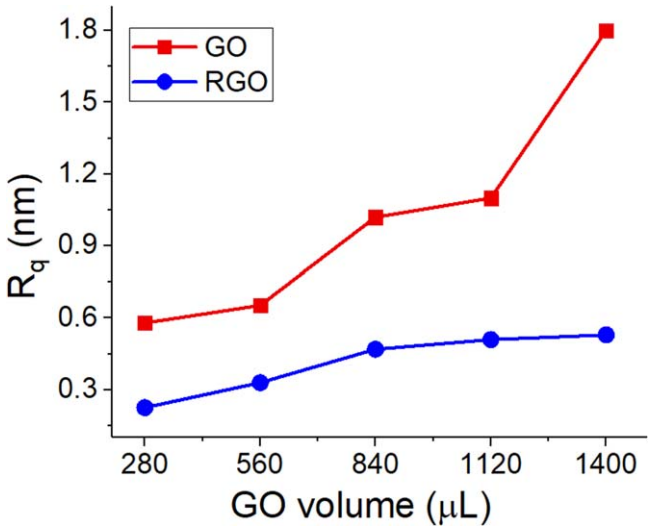

Fig. 3. (Color online) Root mean square roughness (R_q) of the films before (GO) and after (RGO) EtOH annealing with increase of GO loading volume.

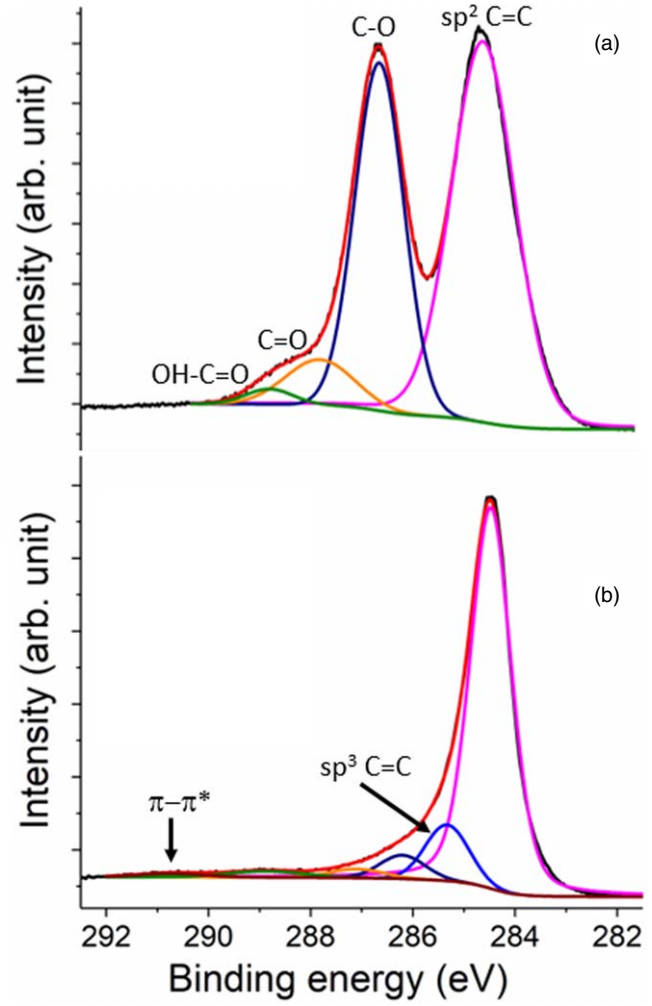

Fig. 4. (Color online) XPS images of GO (a) and RGO (b) at 280 μl loading.

presence of sp^2 C=C (~284.5 eV), C–O in hydroxyl and epoxide groups (~286.6 eV), C=O (~287.8 eV) as well as COOH (~288.9 eV) components. After annealing, the intensity of the peaks corresponding to oxygen-containing functionalities shows a drastic drop, particularly the C–O peak, indicating that basal plane hydroxyl and epoxide groups and interlayer or adsorbed moisture have been removed. The reduced thickness observed in AFM is due to this deoxygenation. The remaining functionalities could be those that are present at defect sites or edges, which are known to be more stable than basal plane functional groups.[8] Two additional peaks are observed in the high-resolution carbon spectrum of the RGO film at 285.3 eV and 290.7 eV that can be attributed to sp^3 C–C and C–H bonds, and the π–π^* satellite peak (due to C=C conjugation), respectively. The edge saturation by H atoms resulting in C–H bonds may be from the H_2 in the carrier gas.

Figure 5(a) illustrates the Raman spectra of GO and GO annealed with and without EtOH. Broad D- and G-bands along with a flat D + G region are present in GO due to the highly defected and oxygenated nature. Upon annealing with EtOH, the evolution of the G′-band is clearly observed; this is absent in the sample annealed without EtOH. This is a good indication that restoration has taken place in the presence of EtOH. Additionally, both D- and G-bands have become sharp compared with those in GO and without EtOH. The Raman spectra for the samples prepared with increased GO loading volumes and annealed in the presence of EtOH are presented in Fig. 5(b). The intensity of the G′-band has decreased and the peaks have become broad with increase in the GO loading amount. Unlike in graphite, where the graphene sheets show an ordered AB Bernal stacking behavior, RGO sheets show a disordered stacking behavior caused by spin-coating of GO. If the restoration by EtOH occurs in all the RGO sheets despite the thickness, the G′-peak should not become broader.[25,26] Hence, we believe that the reason for this G′-peak broadening is the effect of EtOH on restoration and it could be limited to the topmost layers. This can be further confirmed by analyzing the effect of EtOH on single-, double-, triple- or multi-layer RGO. Figure A6, available online at stacks.iop.org/JJAP/58/SIIB07/mmedia, shows the Raman spectra of RGO sheets with different numbers of layers annealed under same conditions in the presence of EtOH, where with the increase of RGO sheets or layers the G′-peak becomes broader and the $I_{G'}/I_G$ ratio becomes smaller. However, a noticeable change in these parameters cannot be seen in single-, double- or triple-layer RGO, which indicates that restoration by EtOH can reach up to nearly three layers (from top to bottom); above that the effects lessen. The mobility of EtOH molecules and their pyrolyzed fragments also plays an important role in restoration.[27] Migration of these entities through RGO sheets is perhaps not so efficient at increased thicknesses. Hence, the restoration of lattice defects is better performed at the top layers first and to a small extent at inner sheets. However, to make solid conclusions more experiments and theoretical calculations will be required. Figure 6 depicts the Raman maps taken for I_D/I_G ratios of the samples from 280–1400 μl over a 120 μm × 120 μm area with a step-size increment of 2 μm; the corresponding optical microscope images are shown in Fig. 7. Generally, the I_D/I_G ratio is an indication of defect density.[25] Accordingly, the I_D/I_G ratio of the 280 μl sample is the highest and has decreased with increase in GO loading amount. However, we cannot conclude from this that the defects have been decreased, because the D- and G-bands are broad at higher volumes, as is seen in the Raman spectra.

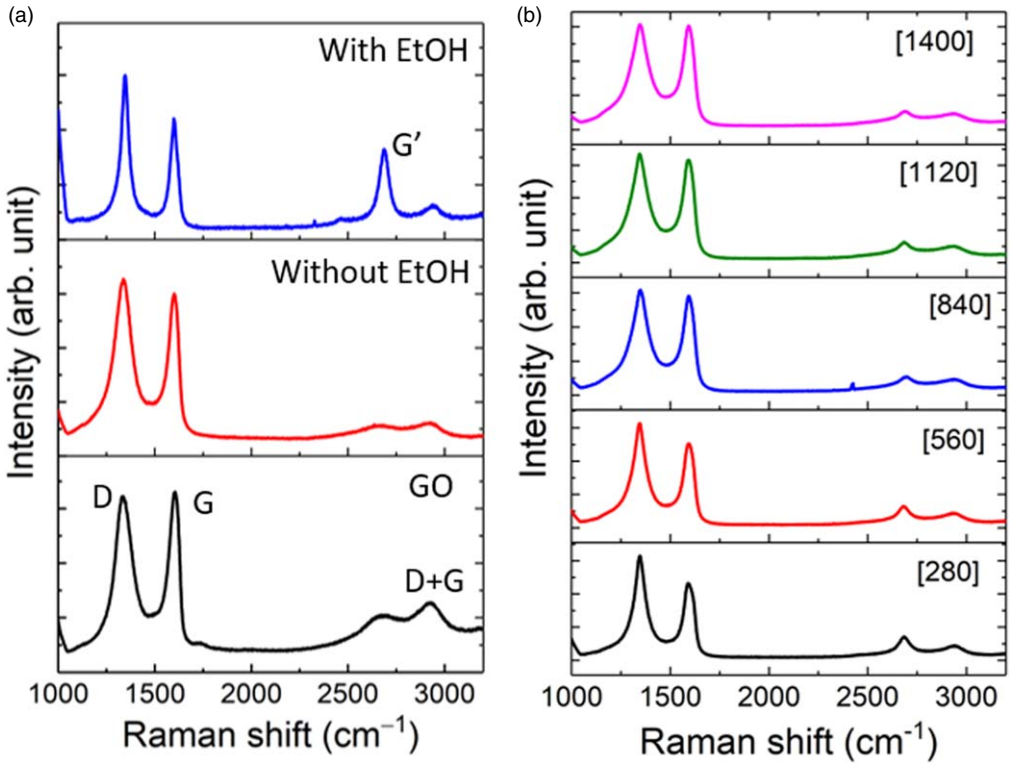

Fig. 5. (Color online) Raman spectra of GO, and GO annealed with and without EtOH for single flakes of GO (a) and Raman spectra of the samples with increased GO loading volumes and annealed in the presence of EtOH (b).

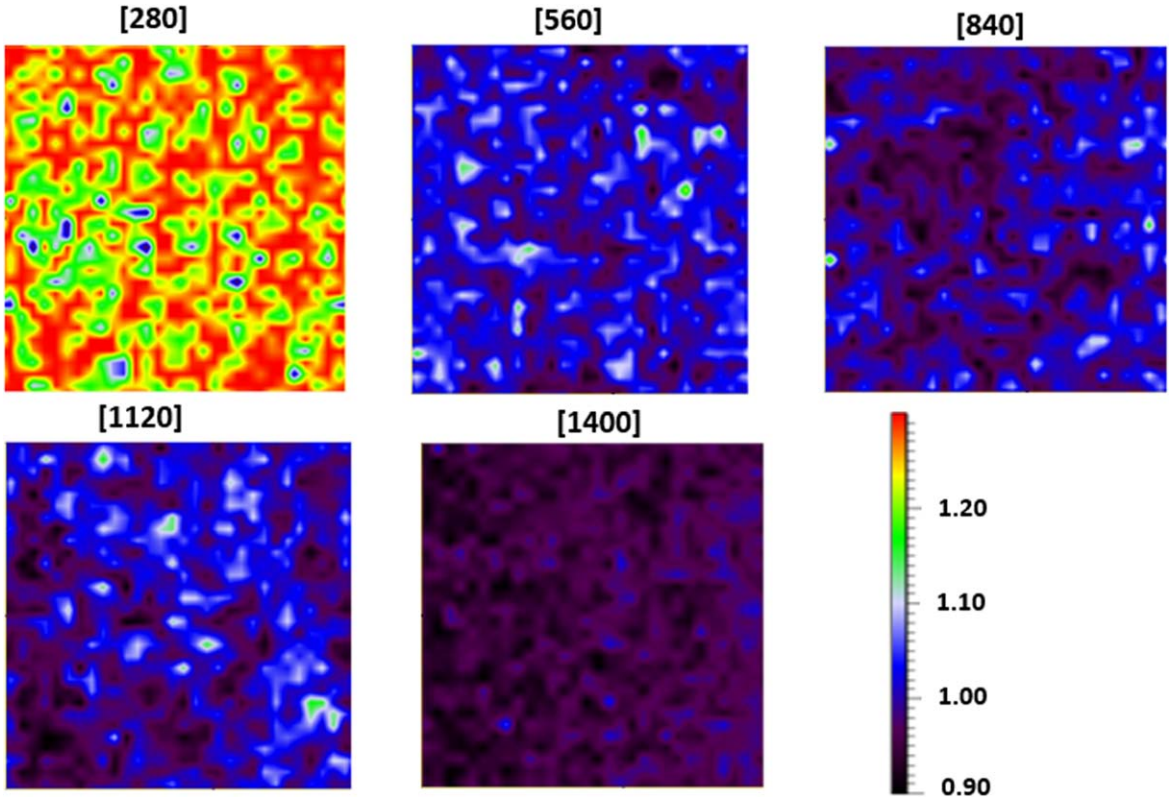

Fig. 6. (Color online) Raman mapping results of the I_D/I_G ratio of the samples from 280–1400 μl GO loading over a 120 μm × 120 μm area (shown at the same vertical scale).

This again affirms the conclusion we made earlier: restoration of lattice defects in bottom layers may have not have properly occurred in thicker samples. As we saw earlier in AFM, at lower GO loading volumes, the substrate is not fully covered while the flakes also appear as three or four monolayers. The high I_D/I_G ratio along with sharp peaks in the 280 μl sample indicate deoxygenation. The red regions with higher I_D/I_G ratio (∼1.3) can be ascribed to monolayers of RGO. With an increase in the number of layers, this ratio decreases (∼1.2).

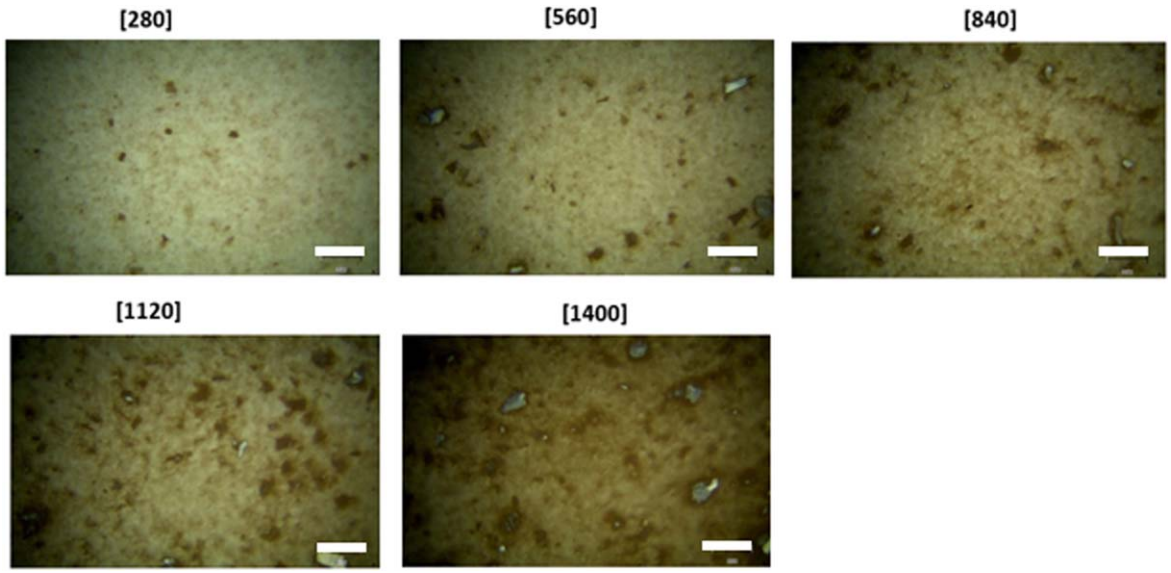

Fig. 7. (Color online) Optical microscopic images (×50 lens) of RGO films fabricated at increasing GO loading volumes (scale bar is 20 μm).

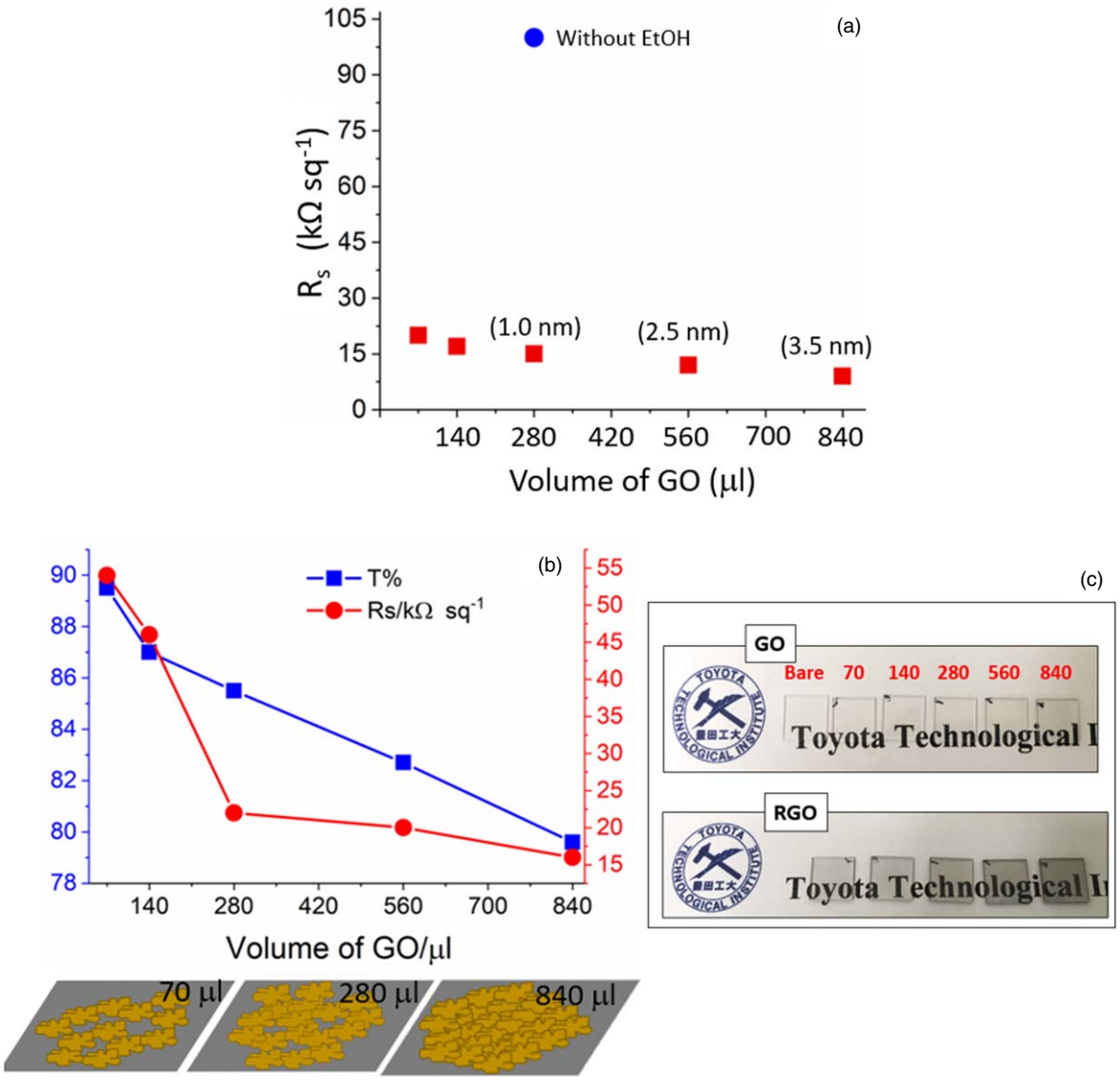

Fig. 8. (Color online) Measurements of the sheet resistance (R_s) and percentage transmittance (T%): R_s of the RGO films on SiO_2/Si substrates (a) (the red and blue symbols are for the samples annealed with and without EtOH, respectively; the thickness of the film after annealing is given within parentheses); (b) R_s and T% of the RGO films on quartz substrates; (c) digital photographs showing the GO and RGO films on quartz substrates with increased GO loading volume.

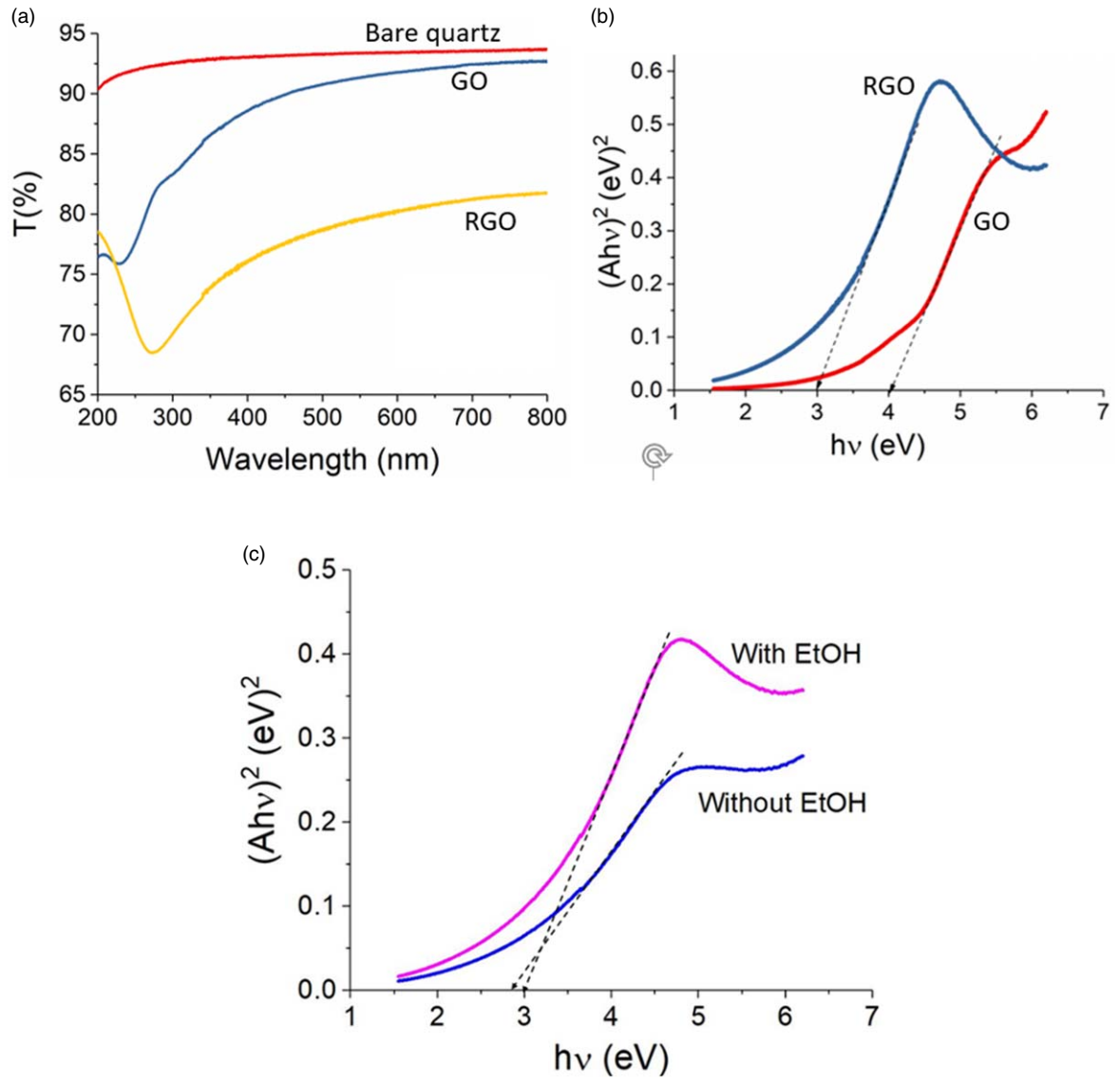

Fig. 9. (Color online) The UV–visible spectra of GO and RGO films on a quartz substrate at 840 μl GO loading and on a bare quartz substrate (a), and the corresponding Tauc plots (b) and the Tauc plots of RGO films prepared with and without EtOH.

The RGO films fabricated on both SiO_2 (50 nm)/Si and quartz substrates with GO loading amounts from 70 to 840 μl were subjected to measurements of R_s by the four-point probe method. Figure 8(a) depicts the R_s of RGO films on a SiO_2/Si substrate fabricated by annealing in the presence of EtOH (in red). For comparison, one sample made without EtOH annealing is also shown (in blue). With the increase in GO loading volume R_s has decreased (from 20 to 9 kΩ sq^{-1}). This can be attributed to the high charge carrier concentration resulting from more restored RGO sheets.[28] In contrast, for the sample annealed without EtOH R_s had a very high value (100 kΩ sq^{-1}) compared with the sample annealed with EtOH at the same GO loading amount (15 kΩ sq^{-1}). This further testifies that EtOH was involved in the restoration of the lattice defects, thereby improving the extended π-conjugated system. The same measurement was carried out for the RGO films fabricated on quartz substrates [see Fig. 8(b)]. In addition to R_s measurements, percentage transmittance (T%) at 550 nm was determined by UV–visible spectroscopy. Although we used the same GO loading amount to fabricate RGO films on both substrates, the R_s values showed noticeable differences, particularly at lower loading amounts (70 and 140 μl). A few assumptions could be made in this regard; firstly, the two substrates have different surface morphologies and/or roughness (the R_q of SiO_2/Si and quartz substrates was found to be 0.28 ± 0.03 nm and 0.44 ± 0.02 nm, respectively), making the deposition of GO flakes on the substrate different. Secondly, the coverage or the distribution of GO flakes on the substrate changes with the increase in GO loading [as shown schematically in Fig. 8(b)]. The two photographs in Fig. 8(c) depict the films fabricated on quartz, before and after annealing, with increasing GO loading. Before annealing, GO films appear transparent due to the insulating properties caused by their highly defective nature. Upon annealing, deoxygenation occurs and most of the defects will be restored. As a result, RGO films appear darker with an increase in GO loading amount as the transmittance decreases. However, when comparing the samples annealed with and without EtOH at the same GO loading amounts, the transparencies of the samples annealed without EtOH were observed to be slightly higher than those of the samples annealed with EtOH (e.g. at 280 μl loading T% values of 81% and 84% were obtained for the samples annealed with and without EtOH, respectively). This is another indication

that restoration has taken place in the presence of EtOH, and when more defects are repaired by EtOH the transparency decreases.[18] Figure 9(a) displays the UV–visible spectra of GO films prepared on a quartz substrate by spin-coating 840 μl of GO before and after annealing and a bare quartz substrate. The GO spectrum has a peak at 230 nm which is attributed to π–π* transition of C=C bonds and a shoulder peak at ~300 nm attributed to n–π* transitions of C=O bonds. In the RGO spectrum, the π–π* peak has redshifted to 272 nm due to the extended double-bond conjugation and the n–π* peak has disappeared due to the removal of C=O groups. Based on these spectra, the Tauc plots[29] were plotted for both GO and RGO [see Fig. 9(b)]. Accordingly, the band gap of both GO and RGO is 4 eV and 3 eV respectively. Hence, GO appears as transparent in the visible and RGO appears darker and becomes conductive. These results are consistent with the values reported in the literature. The band gaps of both GO and RGO can be tuned by controlling the reduction conditions because they largely depend on the number of oxygen-containing groups and lattice defects present in the material.[30,31] Additionally, Tauc plots for samples annealed with and without EtOH were plotted and are shown in Fig. 9(c). A slightly lower band gap for the sample annealed without EtOH was observed (2.8 eV). This trend was the same for other samples (at different GO loadings) annealed without EtOH compared with their counterparts annealed with EtOH. This seems to deviate from the discussion we gave earlier, where in the presence of EtOH lattice defects will be repaired, resulting in highly ordered RGO sheets with a lower band gap. The only difference that can be observed in the UV–visible spectra is the slightly lower *T*% in the sample without EtOH. Hence, a definitive conclusion cannot be given at present.

We note here that we have succeeded in fabricating transparent and conducting RGO films with a total process time of less than 1 h at 800 °C. The works reported so far on RGO-based conducting films have been done at high temperatures or by combining hydrazine-assisted chemical reduction and annealing or by modifying the graphitic structure using polymers or heteroatomic dopants to get better electrical properties. However, in our work the main purpose is to fabricate transparent and conducting RGO films in a roll-to-roll manner with a short process time and at a relatively low temperature. Hence, any structural modifications or doping have not been considered at present.

4. Conclusions

This study demonstrates the possibility of fabricating RGO-based transparent conducting films in a rapid thermal annealing process for the first time at a mild temperature. We have reported that annealing in the presence of EtOH would enhance the electrical properties of the RGO films due to defect repair. Although the obtained sheet resistance values are still too high for many TCE-based applications, this method seems to be promising for fabrication of smart windows or antistatic coatings which do not require higher conductivities. Overall, if this inexpensive and abundant material (RGO) is to be used as a TCE material, substantial improvements in the film fabrication process are necessary to obtain much better electrical properties for commercialization. We also point out the potential use of rapid mild temperature annealing, which is in great demand for industrial-scale fabrication.

Acknowledgments

This work was supported in part by the Strategic Research Foundation Grant-aided Project for Private Universities from MEXT, Japan.

1) S. De and J. N. Coleman, ACS Nano **5**, 2713 (2010).
2) J. K. Wassei and R. B. Kaner, Mater. Today **13**, 52 (2010).
3) K. S. Novoselove, V. I. Falko, L. Colombo, P. R. Gellert, M. G. Schwab, and K. Kim, Nature **490**, 192 (2012).
4) P. Sutter, Nature Mater. **8**, 171 (2009).
5) Z. Juang, C. Wu, A. Lu, C. Su, K. Leou, F. Chen, and C. Tsai, Carbon **48**, 3169 (2010).
6) K. K. H. De Silva, H. Huang, and M. Yoshimura, Appl. Surf. Sci. **447**, 338 (2018).
7) A. Lerf, H. He, M. Forster, and J. Klinowski, J. Phys. Chem. B **102**, 4477 (1998).
8) X. Gao, J. Jang, and H. Nagase, Nanoscale **7**, 2374 (2015).
9) H. A. Becerril, J. Mao, Z. Liu, R. M. Stoltenberg, Z. Bao, and Y. Chen, ACS Nano **2**, 463 (2008).
10) J. Zhao, S. Pei, W. Ren, L. Gao, and H. M. Cheng, ACS Nano **4**, 5245 (2010).
11) M. Savchak et al., ACS Appl. Mater. Interfaces **10**, 3975 (2018).
12) S. Pei and H. M. Cheng, Carbon **50**, 3210 (2012).
13) T. H. Bointon, S. Russo, and M. F. Craciun, IET Circuit Devices Syst. **9**, 403 (2015).
14) R. Rozada, J. I. Paredes, M. J. Lopez, S. Villar-Rodil, I. Cabria, J. A. Alonso, A. Martinez-Alonso, and J. M. D. Tascon, Nanoscale **7**, 2374 (2015).
15) R. K. Singh, R. Kumar, and D. P. Singh, RSC Adv. **6**, 64993 (2016).
16) X. Wang, L. Zhi, and K. Mullen, Nano Lett. **8**, 323 (2008).
17) V. Lopez, R. S. Sundaram, C. Gomez-Navarro, D. Olea, M. Burghard, J. Gomez-Herrero, F. Zamora, and K. Kem, Adv. Mater. **21**, 4683 (2009).
18) Y. Liang, J. Frisch, L. Zhi, H. Norouzi-Arasi, X. Feng, J. P. Rabe, N. Koch, and K. Mullen, Nanotechnology **20**, 434007 (2009).
19) C. Su, Y. Xu, W. Zhang, J. Zhao, A. Liu, X. Tang, C. Tsai, Y. Huang, and L. Li, ACS Nano **4**, 5285 (2010).
20) M. Cheng., R. Yang, L. Zhang, Z. Shi, W. Yang, D. Wang, G. Xie, D. Shi, and G. Zhang, Carbon **50**, 2581 (2012).
21) S. Grimm, M. Schweiger, S. Eigler, and J. Zaumseli, J. Phys. Chem. C **120**, 3036 (2016).
22) K. K. H. De Silva, H. H. Huang, S. Suzuki, R. Badam, and M. Yoshimura, Japan. J. Appl. Phys. **57**, 08NB03 (2018).
23) T. Ishida, Y. Miyata, Y. Shinoda, and Y. Kobayashi, Appl. Phys. Express **9**, 025103 (2016).
24) J. I. Paredes, S. Villar-Rodil, P. Solis-Fernandez, A. Martinez-Alonso, and J. M. D. Tascon, Langmuir **25**, 5957 (2009).
25) S. Eigler, F. Hof, M. Enzelberger-Heim, S. Grimm, P. Muller, and A. Hirsch, J. Phys. Chem. C **118**, 7698 (2014).
26) J. A. Garlow, L. K. Barrett, L. Wu, K. Kisslinger, Y. Zhu, and J. F. Pulecio, Sci. Rep. **6**, 19804 (2016).
27) C. Gong, M. Acik, R. M. Abolfath, Y. Chabal, and K. Cho, J. Phys. Chem. C **116**, 9969 (2012).
28) R. Negishi, M. Akabori, T. Ito, Y. Watanabe, and Y. Kobayashi, Sci. Rep. **6**, 28936 (2016).
29) I. Banerjee, P. Harris, A. Salimian, and A. K. Ray, IET Circuit Devices Syst. **9**, 428 (2015).
30) A. Mathkar, D. Tozier, P. Cox, P. Ong, C. Galande, K. Balakrishnan, A. L. M. Reddy, and P. M. Ajayan, J. Phys. Chem. Lett. **3**, 986 (2012).
31) Abid, P. Sehrawat, S. S. Islam, P. Mishra, and S. Ahmad, Sci. Rep. **8**, 3537 (2018).

